

Towards the linear scaling in DMRG-based tailored coupled clusters: An implementation of DLPNO-TCCSD

Jakub Lang,^{1,2,*} Andrej Antalík,^{1,3,†} Libor Veis,^{1,‡} Jiří Brabec,^{1,§} Örs Legeza,^{4,¶} and Jiří Pittner^{1,**}

¹*J. Heyrovský Institute of Physical Chemistry, Academy of Sciences of the Czech Republic, v.v.i., Dolejškova 3, 18223 Prague 8, Czech Republic*

²*Faculty of Sciences, Charles University, Albertov 6, 128 00 Praha 2, Czech Republic*

³*Faculty of Mathematics and Physics, Charles University, Ke Karlovu 3, 12116, Prague 2, Czech Republic*

⁴*Strongly Correlated Systems "Lendület" Research group,*

Wigner Research Centre for Physics, H-1525, Budapest, Hungary

(Dated: March 26, 2022)

I. INTRODUCTION

Since its introduction to quantum chemistry¹, the coupled cluster (CC) approach has become one of the most widely used methods for the accurate calculations of dynamic correlation. It offers numerous favorable properties, such as compact description of the wave function, size-extensivity, invariance to rotations within occupied or virtual orbital subspaces and also a systematic hierarchy of approximations converging towards the full configuration interaction (FCI) limit². For instance, the CCSD(T) method³, which includes connected single-, double- and perturbative triple excitations, is notoriously referred to as the gold standard of quantum chemistry².

Although the CC method performs well for single reference molecules, it becomes fairly inaccurate or breaks down completely for systems with strongly correlated electrons. Such systems are multireference in nature since they include quasi degenerate frontier orbitals, which are common during dissociation processes, in diradicals, or compounds containing transition metals. Over the years, numerous efforts to generalize the CC ansatz and thus overcome this drawback gave rise to a broad family of multireference CC methods (MRCC)^{4–6}.

One such approach, aiming to include static correlation in the CC scheme is to employ a different method like complete active space self-consistent field (CASSCF) or multireference configuration interaction (MRCI) in order to extract the information about the most important excitations^{7–29}. The retrieved information can be then introduced to a CC calculation as an external correction. One of such methods is tailored CC with single and double excitations (TCCSD) proposed by Kinoshita et al.¹⁴, which draws on the split-amplitude ansatz, in which the amplitudes corresponding to single and double excitations are split into two parts. The active part is treated by complete active space configuration interaction (CAS-CI) and external amplitudes are iterated using the standard CCSD framework. We recently extended this approach by using the density matrix renormalization group (DMRG) method to obtain the active space amplitudes³⁰.

The DMRG method, which originated in solid-state physics^{31–33}, is nowadays well established in quantum chemistry for the treatment of strongly correlated systems^{34–42}. As a numerical approximation to full con-

figuration interaction (FCI), it can handle significantly larger active spaces compared to the conventional method. However, even then the prohibitive scaling does not allow to include dynamic correlation and it is therefore necessary to employ some "post-DMRG" procedure. Many different attempts has been made to tackle this limitation for example DMRG-CASPT2⁴³, Cholesky decomposition DMRG-NEVPT2⁴⁴, DMRG-icMRCI⁴⁵, canonical transformation⁴⁶, matrix product state (MPS) based formulation of multireference perturbation theory⁴⁷, DMRG pair-density functional theory⁴⁸, and also our aforementioned CC tailored by MPS wave functions (DMRG-TCCSD)^{30,49,50}.

Even though the DMRG-TCCSD method offers a reasonably efficient treatment of both static and dynamic correlation⁵¹, its applications to larger systems is hampered by the unfavorable scaling of the CCSD part of the calculation. With such a steep scaling, even massive parallelization itself is not sufficient to make the method applicable to molecules with hundreds of atoms. A well known way to overcome the steep scaling of conventional coupled cluster method, first introduced by Pulay^{52,53}, is to exploit the locality of the electron correlation. For non-metallic systems, the electron correlation has a short range character, decaying as R^{-6} with the interelectronic distance R . Therefore, in the basis of localized orbitals the Hamiltonian matrix becomes sparse for large systems.

The occupied orbital space can be localized using Foster-Boys⁵⁴, Pipek-Mezey method⁵⁵, or the intrinsic bond orbital approaches⁵⁶. For the virtual space, various possibilities have been used. In the first works of Pulay and Sæbø, projected atomic orbitals (PAOs) were employed^{57,58}. These were also used by Werner and Schütz in the local CC method^{59–63}. Each localized occupied orbital is assigned a domain of spatially close PAOs, which are obtained by projecting out the occupied orbital components from the atomic orbitals. As such, the PAOs are local by construction. The pairs of occupied orbitals are subsequently classified according to their real space distance and subsequently treated at the coupled cluster level (strong pairs), perturbative level (weak and distant pairs), or neglected altogether (very distant pairs). Using this approach, linear scaling was obtained.

Another group of local approaches is based on the concept of dividing a large system into smaller subsystems, and performing calculations for each of the sub-

systems. These approaches include, among many others, the divide-expand-consolidate method^{64,65}, the divide-and-conquer method⁶⁶, the incremental method⁶⁷, the local natural orbital method⁶⁸, and the fragment molecular orbital method⁶⁹. A closely related cluster-in-molecule method⁷⁰ is based on decomposition of the energy formula into contributions corresponding to individual occupied orbitals. However, possibly the most effective way to truncate the virtual space is to use pair natural orbitals (PNOs), i.e. natural orbitals specific for each pair of occupied orbitals, which are known to provide the most compact parameterization of the virtual space. The PNOs were first used in the 1960s by Edmiston and Kraus⁷¹ and later by Meyer^{72–76}, Ahlrichs and Kutzelnigg^{77,78}. The use of PNOs was revived in 2009 in combination with the use of localized occupied orbitals in the local pair natural orbital (LPNO) variants of CEPA and CCSD approaches^{79–82}. In the more advanced domain based local pair natural orbital (DLPNO) methods^{83–86}, the PNOs were expanded as a linear combination of PAOs in the pair-domain and used also for the connected singles excitations, in order to remove the bottlenecks of LPNO methods. Thus, the DLPNO-CCSD achieves genuine linear-scaling unlike the LPNO variants⁸⁶. The PNO approaches have many desirable properties. They provide a very compact description of the virtual space. Therefore, it is computationally feasible to use sufficiently large domains of PAOs which would be too costly for purely-PAO-based approaches. Only a limited number of cut-off parameters is used and they do not involve distances in real space. Therefore, the dependence of the calculated correlation energy on the values of cut-off parameters is smooth and the method can be used as a black box. The resulting DLPNO-CCSD method is applicable to systems with hundreds of atoms and thousands of basis functions, so that the preceding SCF calculation can become computationally more expensive than the correlation treatment.

Nowadays, the PNO-based approaches are developed in number of groups including Werner^{87–90} and Hättig^{91–93} and widely applied to various systems of chemical interest^{94–103}. Apart from single-reference methods, the LPNO and DLPNO methodologies were also successfully applied to multireference CC techniques^{104–107}

II. THEORY AND IMPLEMENTATION

A. DMRG-based Tailored Coupled Clusters

The tailored coupled cluster method, which belongs to the class of externally corrected methods, employs the split-amplitude wave function ansatz proposed by Kinoshita et al.¹⁴

$$|\Psi_{\text{TCC}}\rangle = e^T |\Phi_0\rangle = e^{T_{\text{ext}} + T_{\text{CAS}}} |\Phi_0\rangle = e^{T_{\text{ext}}} e^{T_{\text{CAS}}} |\Phi_0\rangle, \quad (1)$$

where the cluster operator T is split into two parts: T_{CAS} which contains the active amplitudes obtained from an external calculation and T_{ext} which contains the external amplitudes, with $|\Phi_0\rangle$ being the reference wave function.

In our implementation, we employed the DMRG method to obtain the active amplitudes. Using the DMRG algorithm we first optimize the wave function, which is provided in the matrix product state (MPS) form

$$|\Psi_{\text{MPS}}\rangle = \sum_{\{\alpha\}} \mathbf{A}^{\alpha_1} \mathbf{A}^{\alpha_2} \cdots \mathbf{A}^{\alpha_k} |\alpha_1 \alpha_2 \cdots \alpha_k\rangle, \quad (2)$$

where $\alpha \in \{ |-\rangle, |\downarrow\rangle, |\uparrow\rangle, |\downarrow\uparrow\rangle \}$ and \mathbf{A}^{α_i} are MPS matrices. These are then contracted to obtain CI coefficients for single and double excitations $C^{108,109}$. Using the relations between CI and CC coefficients

$$T_{\text{CAS}}^{(1)} = C^{(1)}, \quad (3)$$

$$T_{\text{CAS}}^{(2)} = C^{(2)} - \frac{1}{2}[C^{(1)}]^2, \quad (4)$$

we are able to acquire their respective amplitudes, which are subsequently introduced into the CC calculation. At this point, these active amplitudes are kept frozen, while the remaining amplitudes T_{ext} are optimized by solving the equations

$$\langle \Phi_i^a | H e^{T_{\text{ext}}} e^{T_{\text{CAS}}} |\Phi_0\rangle_c = 0 \quad \{i, a\} \not\subset \text{CAS} \quad (5)$$

$$\langle \Phi_{ij}^{ab} | H e^{T_{\text{ext}}} e^{T_{\text{CAS}}} |\Phi_0\rangle_c = 0 \quad \{i, j, a, b\} \not\subset \text{CAS} \quad (6)$$

analogously to the standard CCSD equations. This way, the active amplitudes account for static correlation and by optimizing the external amplitudes, we are able to recover the remaining dynamic correlation.

B. The DLPNO Approach for DMRG-TCCSD

As with different DLPNO methods, the whole procedure starts with the localization of the internal orbitals. In the case of TCC, we separately localize the external occupied orbitals and split-localize the orbitals within the active space. Using the idea of Werner et al.^{110,111}, we transform the virtual orbitals by projecting out the localized occupied and active orbitals

$$|\tilde{\mu}\rangle = \sum_i \left(1 - |i\rangle\langle i|\right) |\mu\rangle, \quad (7)$$

where $|\mu\rangle$ is the original atomic orbital, while the summation runs over localized occupied and active virtual orbitals. Finally, these are normalized

$$|\tilde{\mu}\rangle \leftarrow \frac{|\tilde{\mu}'\rangle}{\sqrt{\langle \tilde{\mu}' | \tilde{\mu}' \rangle}}, \quad (8)$$

in order to obtain the final set of PAOs.

Compared to the single-reference DLPNO-CCSD, the tailored indices are formally treated as singly occupied orbitals during the creation of domains and share the same domain.

Next, it is necessary to ensure that every tailored occupied pair (i.e. with both active indices) will automatically

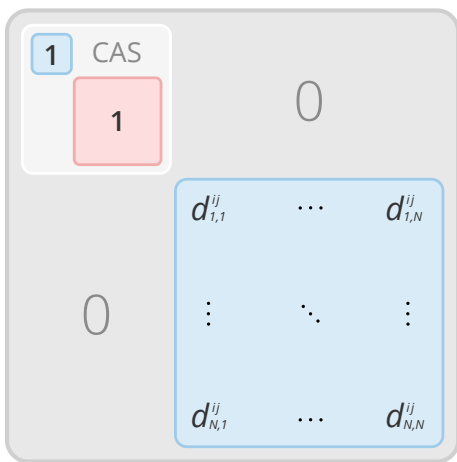


FIG. 1. An illustration of an PAO/PNO transformation matrix for an active pair ij in DLPNO-TCC. The original transformation matrix \mathbf{d}^{ij} , with N being the number of PNOs, is enlarged by an identity matrix of size N_{CAS} , which is formally composed of two blocks corresponding to singly occupied (blue) and virtual orbitals (red) included in the active space.

survive the dipole prescreening. The occupied pairs belonging to the active space are set to automatically survive MP2 energy screening.

Subsequently, the pair density is constructed from nonredundant PAOs, which do not contain any explicit information about the tailored CAS space, and is diagonalized to obtain PNOs. This PNO expansion is then truncated based on the second cut-off parameter T_{CutPNO} . Only PNOs with occupation numbers larger than T_{CutPNO} are kept and the remaining orbitals are discarded. The final PAO/PNO transformation matrices are then obtained by enlarging the former transformation matrix S^{ij} by adding unit matrices corresponding to active orbitals (i.e. singly occupied and tailored virtual orbitals) to the diagonal, see Figure 1.

The resulting equation for singly excited amplitudes (5) now becomes

$$\langle \Phi_{\bar{a}} | H e^{\bar{T}_{\text{ext}}^{(1)} + \bar{T}_{\text{ext}}^{(2)}} e^{T_{\text{CAS}}} | \Phi_0 \rangle_c = 0 \quad \{i, a\} \notin \text{CAS}, \quad (9)$$

where \bar{a} indicate the PNO basis. Similarly, the equation for doubly excited amplitudes (6)

$$\langle \Phi_{\bar{a}\bar{b}} | H e^{\bar{T}_{\text{ext}}^{(1)} + \bar{T}_{\text{ext}}^{(2)}} e^{T_{\text{CAS}}} | \Phi_0 \rangle_c = 0 \quad \{i, j, a, b\} \notin \text{CAS}, \quad (10)$$

with the active amplitudes formally in PNO basis. Except “freezing” the active amplitudes, these equations are identical to single-reference DLPNO-CCSD as implemented in Orca⁸⁶

III. COMPUTATIONAL DETAILS

The DMRG calculations were performed by Budapest QC-DMRG code¹¹². The LPNO-TCCSD method was implemented in ORCA program package¹¹³, which was also used to prepare the orbitals.

In case of TME, we used CASPT2(6,6)/cc-pVTZ geometries for seven values of the dihedral angle from our previous work⁵¹. The orbitals were prepared by CASSCF(6,6) calculation with the active space containing six $2p_z$ orbitals on carbon atoms.

In case of oxo-Mn(Salen), we used the singlet CASSCF(10,10)/6-31G* optimized geometry by Ivanic et al.¹¹⁴. The orbitals were optimized using the DMRG-CASSCF method^{115–117} in Dunning’s cc-pVXZ $X \in \{D, T, Q\}$ basis sets^{118–120}. The optimization was carried out with fixed bond dimension $M = 1024$ for the smaller CAS(28,22) and $M = 2048$ for CAS(28,27). The composition of these active spaces is discussed further in the Results section. The orbitals were then split-localized using the Pipek-Mezey algorithm⁵⁵ in the following orbital subspaces: internal, active doubly occupied, active singly occupied and active virtual.

The orbitals for DMRG were ordered using the Fiedler method^{121,122} combined with some manual adjustments. All DMRG runs were initialized by CI-DEAS procedure^{41,123}. We employed the dynamical block state selection (DBSS) procedure^{124,125} to control the accuracy of the larger oxo-Mn(Salen) calculations with the truncation error criterion set to 10^{-6} . This resulted in block dimension varying between 1000 up to 2500 block states for CAS(28,22) and up to 8200 in case of CAS(28,27). The convergence threshold was set to energy difference between two subsequent sweeps smaller than 10^{-6} a.u.

The core electrons were kept frozen throughout all coupled cluster calculations. Auxiliary basis sets cc-pVQZ/C and cc-pV6Z/C were used for the resolution of the identity approximation for oxo-Mn(Salen) and TME respectively^{126,127}. The default DLPNO cut-off parameters were set to $T_{\text{CutPNO}} = 3.33 \cdot 10^{-7}$, $T_{\text{CutPairs}} = 10^{-4}$ and $T_{\text{CutMKN}} = 10^{-3}$ and these were used unless otherwise stated. The production runs of oxo-Mn(Salen) were performed with ORCA’s TightPNO settings i.e. the cut-off parameters set to $T_{\text{CutPNO}} = 10^{-7}$, $T_{\text{CutPairs}} = 10^{-5}$ and $T_{\text{CutMKN}} = 10^{-4}$. For calculations which purpose was to estimate the dependence of DLPNO-TCCSD energies on these parameters, one parameter was varied with remaining parameters fixed to the default value. We assess the amount of retrieved correlation energy by LPNO approach with reference to a DMRG-TCCSD energy calculated with the canonical TCCSD implementation.

IV. RESULTS AND DISCUSSION

A. Tetramethyleneethane

Although small, the tetramethyleneethane molecule is a challenging system due to its complex electronic structure. To correctly describe the character of its singlet state, one needs to employ a theory with a balanced description of both static and dynamic correlation combined with a reasonably large basis set. This is the reason, why it often serves as a benchmark system for multireference methods^{51,128–132}. Moreover, it was already a subject

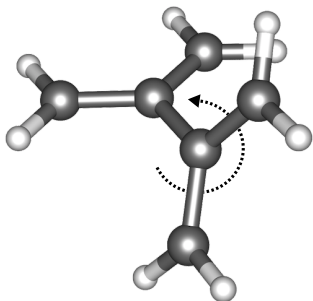


FIG. 2. Dihedral rotation of tetramethylenethane.

of our previous study with the canonical DMRG-TCCSD method⁵¹, so it only seems natural to use this system to test the performance of the LPNO approach to TCCSD. For this purpose, we investigate the behavior of the approximation with respect to different geometries corresponding to the rotation about its central C–C bond (see Figure 2) and different values of the cut-off parameters.

We only present results for a small active space corresponding to six electrons in six 2p orbitals. This decision followed an effort to perform the performance evaluation on three active spaces of different sizes. However, because of the small localization subspaces stemming from a small number of occupied orbitals, many orbitals remained rather delocalized. This resulted in large numbers of PNOs necessary to maintain the accuracy, even for looser cut-off parameters, which ultimately rendered the DLPNO approximation useless due to its low efficiency. Therefore, we compare the performance of DLPNO-TCCSD and LPNO-TCCSD with different sized active spaces on oxo-Mn(Salen), which is better suited for this purpose.

The benchmarks were performed only for T_{CutPairs} and T_{CutPNO} cut-off parameters as T_{CutDO} does not affect the results unless extremely small cut-off value is chosen, which is in correspondence with results from previous studies^{86,106,107}.

With respect to T_{CutPNO} (see Figure 3), the DLPNO-TCC shows a faster convergence to the canonical value than LPNO-TCC. Furthermore, DLPNO-TCC is able to describe both spin states equally well and the difference of the recovered correlation energy is less than 0.01%. In comparison, the LPNO-TCC recovered correlation energy for the triplet state is worse by 0.1% than for the singlet state. This discrepancy in LPNO-TCC can be explained by the missing terms in the UHF-LPNO formalism. On the other hand, DLPNO does not suffer from this problem, as is numerically confirmed here. At the default cutoff values, DLPNO-TCC extracts more than 99.91% of the canonical correlation energy.

The results for T_{CutPairs} cut-off parameter are presented in Figure 3. Both methods converge in a similar fashion, but DLPNO-TCC recovers about 0.1% more correlation energy than LPNO-TCC for the singlet state and more than 0.3% for the triplet state.

Furthermore, the non-parallelity error is given in Figure 4. For the default threshold, the NPE is only 0.16 kcal/mol

for singlet and 0.17 kcal/mol for the triplet state; for lower values of T_{CutPNO} it decreases to 0.13 and 0.1 kcal/mol, respectively.

From the chemical point of view, the most interesting property is the behavior of the singlet-triplet gap with respect to the cut-off parameters. It was shown in literature¹³³ that the bigger CAS space and basis set is required to qualitatively assess the singlet-triplet gap of TME. Therefore, the following E_{ST} can only be seen as a benchmark to test the performance of DLPNO-TCC with respect to the canonical method. The results for singlet-triplet gap of TME calculated by DLPNO-TCC are presented in Figure 5. For the cut-off parameter T_{CutPNO} , the DLPNO-TCC achieves an accuracy of sub kJ/mol already at $T_{\text{CutPNO}} = 1.0 \times 10^{-6}$.

B. oxo-Mn(Salen)

The oxo-Mn(Salen) molecule has been a subject of numerous computational studies motivated mainly by its role in catalysis of the enantioselective epoxidation of unfunctional olefins^{134,135}. Moreover, its closely lying singlet and triplet states pose a considerable challenge for multireference methods. Over the years, several multireference studies has been published^{114,136,137}, some of which employed the DMRG method^{138–140} and recently the first DMRG results with dynamic correlation treatment were presented^{30,141}. Our aim was to contribute to these efforts by exploring the effect of the active space and basis set dependence. on the character of the ground state. With our LPNO implementation we were able to study the effect of dynamic correlation up to the quadruple- ζ basis set. This would not be possible without the DLPNO approximation, since the cc-pVQZ basis for this systems amounts to 1178 basis functions.

In order to assess the accuracy of the DLPNO-TCCSD method with respect to active spaces of different size and investigate the different ground states reported at the CASSCF level, we selected two active spaces. In accordance with the study by Wouters et al.¹³⁸, the smaller CAS(28,22) consists of ten π orbitals on equatorial conjugated rings (C, N and O atoms), five 3d orbitals on Mn, three 2p orbitals on the axial O atom and four 2p orbitals on equatorial N and O atoms forming σ bonds with the Mn atom. On top of these, we added extra five orbitals on Mn resulting in CAS(28,27), namely $4d_{xy}$, $4d_{yz}$, and $4p_x$, $4p_y$ and $4s$, which form σ^* bonds with Mn. The effect of inclusion of these particular orbitals is discussed further in the text. On top of that, we also tried to add 3p orbitals on Cl to the active space, since these were included in some of the studies^{30,139} but based on the results of entanglement analysis (one-orbital entropies) we concluded that their effect was negligible.

Firstly, the percentage of the recovered correlation energy (with respect to canonical TCC) was assessed with respect to the cut-off parameter T_{CutPairs} . The curve shows the same trend as in previous cases of DLPNO-CC studies and quickly converges. At the value of $T_{\text{CutPairs}} =$

1.0×10^{-5} the curve is already converged. However, this value is an order of magnitude lower than the default $T_{\text{CutPairs}} = 1.0 \times 10^{-4}$. This suggests that to correctly describe oxo-Mn(salen), a tighter threshold is crucial since the energy difference between the two cut-off values is about 0.16%. Furthermore, the results show that the behavior of different CAS spaces is similar.

The dependence on the cut-off parameter T_{CutPNO} is presented in Figure 8. Looking back at the T_{CutPairs} parameter, two curves were calculated: a) with default $T_{\text{CutPairs}} = 1.0 \times 10^{-4}$ cut-off parameter denoted as *NormalPairs* and presented in Figure 8a; b) tighter one in Figure 8b with $T_{\text{CutPairs}} = 1.0 \times 10^{-5}$ denoted as *TightPairs*. As can be seen from Figure 8a, the curve for NormalPairs converges to 100% but when very conservative T_{CutPNO} values are chosen, the recovered correlation energy is more than 100%. This is caused by overcompensation of the neglected pairs with the MP2 pair energy. Therefore, the use of the slightly tighter cut-off T_{CutPairs} is required. For the NormalPairs curve, the percentage of the recovered correlation energy is more than 99.86% for CAS(28,22) and 99.80% for CAS(28,27). These results are slightly better than those of LPNO (99.85% and 99.78% respectively). For the TightPairs curve, the results are worse as there is less overestimation of pair energy from MP2, the recovered percentage of correlation energy is also smaller. The resulting values are thus 99.80% and 99.76%, respectively. However, now the curve converges to 100% even for conservative values.

At the default values, the error of DLPNO-TCCSD(28,22) is 0.60 kcal/mol, which is within the chemical accuracy. When the TightPNO settings are used, this error lowers to the value of 0.44 kcal/mol. For CAS(28,27), the errors are 0.54 kcal/mol at NormalPNO level and 0.34 kcal/mol at TightPNO (cf. Figure 9).

Surprisingly, the errors for bigger CAS space are smaller than for CAS(28,22), while the opposite was observed for LPNO-TCC. This was accredited to the missing terms in the LPNO methods, while the DLPNO method contains all the terms in CCSD equations and thus does not suffer from this drawback.

As the percentage of the recovered energy is smaller, the error of the singlet-triplet gap with respect to canonical value is also smaller cf. Table II. Moreover, the error converges to zero with lowering T_{CutPNO} for both curves as can be seen from Figure 9.

When comparing the two CAS spaces, the triplet state energy is basically unchanged when additional double-shell d orbitals are added. On the other hand, the singlet state is stabilized by the inclusion of double-shell d orbitals. Nonetheless, the predicted ground state is always triplet, irrespective to the CAS space.

Interestingly, the S-T gap increases about 0.5 kcal/mol when the bigger basis set is employed. However, when the TightPNO setting is used, the barrier again lowers to a value close to the one in cc-pVDZ. Cc-pVQZ result is close to the cc-pVDZ one again. For DLPNO-CCSD(28,27), the gap gradually lowers to 3.1 kcal/mol and at the cc-pVQZ

level both PNO settings provide the same value.

While DLPNO-TCCSD obtained a higher percentage of the correlation energy, LPNO-TCCSD provided slightly better S-T gap error with respect to the canonical method due to a fortunate cancellation of errors. Nonetheless, DLPNO-TCCSD is in the chemical accuracy range.

Furthermore, DLPNO-TCCSD results are in an excellent agreement with results from NEVPT2(28,22) in cc-pVQZ basis.

V. CONCLUSIONS

We introduced a new version of DMRG-TCCSD method, which employs the domain-based local pair natural orbital approach. The method has been implemented in ORCA presently at the singles and doubles level.

We performed accuracy assessment of the method employing two systems, which were previously studied by the canonical TCCSD method. Regarding tetramethylenethane, we were able to retrieve over 99.9% of the canonical correlation energy, while using the default settings of cut-off parameters. For oxo-Mn(Salen), the amount of retrieved correlation was dependent on the size of the active space used, ranging from 99.8% for the larger CAS(28,27) to 99.9% for smaller CAS(28,22), which is an improvement about 0.2% with respect to LPNO-TCCSD. Using the default settings resulted in singlet-triplet gap being off by 0.5-0.6 kcal/mol and with tighter cut-offs only 0.3-0.4 kcal/mol compared to canonical calculation. This results are slightly worse than those of LPNO-TCCSD by 0.1 kcal/mol and 0.3 kcal/mol, respectively. We believe that this is due to a fortunate cancellation of errors in LPNO-TCCSD as DLPNO-TCCSD results for other systems are better and DLPNO-TCCSD does not neglect any terms.

Regarding the future of the method, we would like to implement the perturbative triple correction to DLPNO-TCCSD, which we hope to further enhance capabilities of the method and also we have started to work on EOM-TCCSD and DLPNO-EOM-TCCSD, which allows to describe excited states.

ACKNOWLEDGMENT

We would like to thank Prof. Frank Neese for providing us with access to ORCA source code, as well as for helpful discussions, Dr. Frank Wennmohs for technical assistance with the ORCA code and Dr. Ondřej Demel for helpful discussions.

This work has been supported by the Czech Science Foundation (Grants No. 16-12052S and 18-18940Y), Czech Ministry of Education, Youth and Sports (Project No. LTAUSA17033) and by The Ministry of Education, Youth and Sports from the Large Infrastructures for Research, Experimental Development and Innovations project „IT4Innovations National Supercomputing Center – LM2015070“.

TABLE I. The singlet and triplet energies of oxo-Mn(salen) $E + 2251$ in atomic units and the difference $\Delta E_{S-T} = E(^1A) - E(^3A)$ in kcal/mol. Results for different active spaces and in various basis sets.

	cc-pVDZ			cc-pVTZ			cc-pVQZ		
	1A	3A	ΔE_{T-S}	1A	3A	ΔE_{T-S}	1A	3A	ΔE_{T-S}
TCCSD(34,25) ^{142a}	-2.7273	-2.7330	3.6						
MRLCC(28,22) ¹⁴¹	-3.2830	-3.2600	-14.4	-4.1303	-4.1310	0.5			
NEVPT2(28,22) ¹⁴¹	-3.0109	-2.9990	-7.4	-3.8437	-3.8463	1.6	-4.1441	-4.1481	2.4
LPNO-TCCSD(28,22) ¹⁴³	-3.1455	-3.1554	6.2	-3.9698	-3.9798	6.3	-4.2479	-4.2578	6.3
DLPNO-TCCSD(28,22)	-3.1487	-3.1596	6.9	-3.9722	-3.9837	7.3	-4.2490	-4.2595	6.9
LPNO-TCCSD(28,27) ^{b143}	-3.1491	-3.1550	3.7	-3.9749	-3.9798	3.1	-4.2531	-4.2578	2.9
DLPNO-TCCSD(28,27) ^b	-3.1525	-3.1590	4.1	-3.9780	-3.9843	4.0	-4.2563	-4.2612	3.1

^a These values were obtained with split-localized ROHF orbitals.

^b Results with TightPNO settings.

TABLE II. Singlet-triplet energy [kcal/mol] gap for oxo-Mn(salen). NormalPNO means the $T_{\text{CutPairs}} = 1.0 \times 10^{-4}$, $T_{\text{CutPNO}} = 3.33 \times 10^{-7}$, while for TightPNO $T_{\text{CutPairs}} = 1.0 \times 10^{-5}$ and $T_{\text{CutPNO}} = 1.0 \times 10^{-7}$

	Basis set	NormalPNO	TightPNO	Canonical
DLPNO-TCCSD(28,22)	cc-pVDZ	6.86	6.70	6.26
	cc-pVTZ	7.27	6.97	-
	cc-pVQZ	6.92	6.59	-
DLPNO-TCCSD(28,27)	cc-pVDZ	4.28	4.08	3.74
	cc-pVTZ	3.95	4.00	-
	cc-pVQZ	3.13	3.11	-

* jakub.lang@jh-inst.cas.cz

† andrej.antalik@jh-inst.cas.cz

‡ libor.veis@jh-inst.cas.cz

§ jiri.brabec@jh-inst.cas.cz

¶ legeza.ors@wigner.mta.hu

** jiri.pittner@jh-inst.cas.cz

¹ Čížek, J. *J. Chem. Phys.* **1966**, *45*, 4256.

² Gauss, J. In *The Encyclopedia of Computational Chemistry*; v. R. Schleyer, P., Allinger, N. L., Clark, T., Gasteiger, J., Kollman, P. A., Schaefer III, H. F., Scheiner, P. R., Eds.; Wiley: Chichester, 1998; pp 615–636.

³ Raghavachari, K.; Trucks, G. W.; Pople, J. A.; Head-Gordon, M. *Chem. Phys. Lett.* **1989**, *157*, 479.

⁴ Bartlett, R. J.; Musial, M. *Rev. Mod. Phys.* **2007**, *79*, 291.

⁵ Tew, D. P.; Hättig, C.; Bachorz, R. A.; Klopper, W. In *Recent Progress in Coupled Cluster Methods*; Čársky, P., Paldus, J., Pittner, J., Eds.; Springer Science: New York, 2010; p 535.

⁶ Lyakh, D. I.; Musial, M.; Lotrich, V. F.; Bartlett, R. J. *Chem. Rev.* **2012**, *112*, 182–243.

⁷ Li, X.; Paldus, J. *J. Chem. Phys.* **1997**, *107*, 6257.

⁸ Li, X.; Paldus, J. *J. Mol. Struct.: THEOCHEM* **2001**, *547*, 69–81.

⁹ Li, X.; Paldus, J. *J. Chem. Phys.* **2001**, *115*, 5759–5773.

¹⁰ Li, X.; Paldus, J. *J. Chem. Phys.* **2001**, *115*, 5774–5783.

¹¹ Paldus, J.; Planelles, J. *Theor. Chim. Acta* **1994**, *89*, 13.

¹² Piecuch, P.; Tobola, R.; Paldus, J. *Phys. Rev. A* **1996**, *54*, 1210.

¹³ Li, X.; Peris, G.; Planelles, J.; Rajadell, F.; Paldus, J. J.

Chem. Phys. **1997**, *107*, 90.

¹⁴ Kinoshita, T.; Hino, O.; Bartlett, R. J. *J. Chem. Phys.* **2005**, *123*, 074106.

¹⁵ Lyakh, D. I.; Lotrich, V. F.; Bartlett, R. J. *Chem. Phys. Lett.* **2011**, *501*, 166–171.

¹⁶ Melnichuk, A.; Bartlett, R. J. *J. Chem. Phys.* **2012**, *137*, 214103.

¹⁷ Melnichuk, A.; Bartlett, R. J. *J. Chem. Phys.* **2014**, *140*, 064113.

¹⁸ Piecuch, P.; Oliphant, N.; Adamowicz, L. *J. Chem. Phys.* **1993**, *99*, 1875–1900.

¹⁹ Piecuch, P.; Adamowicz, L. *J. Chem. Phys.* **1994**, *100*, 5792–5809.

²⁰ Adamowicz, L.; Piecuch, P.; Ghose, K. B. *Mol. Phys.* **1998**, *94*, 225–234.

²¹ Piecuch, P. *Mol. Phys.* **2010**, *108*, 2987–3015.

²² Piecuch, P.; Kowalski, K.; Pimienta, I. S. O.; McGuire, M. J. *Int. Rev. Phys. Chem.* **2002**, *21*, 527–655.

²³ Piecuch, P.; Kowalski, K.; Pimienta, I. *Int. J. Mol. Sci.* **2002**, *3*, 475–497.

²⁴ Kowalski, K.; Piecuch, P. *J. Chem. Phys.* **2002**, *116*, 7411–7423.

²⁵ WŁoch, M.; Lodriguito, M. D.; Piecuch†, P.; Gour, J. R. *Mol. Phys.* **2006**, *104*, 2149–2172.

²⁶ Lodriguito, M. D.; Kowalski, K.; WŁoch, M.; Piecuch, P. *J. Mol. Struct.: THEOCHEM* **2006**, *771*, 89–104.

²⁷ Piecuch, P.; Kowalski, K.; Pimienta, I. S. O.; Fan, P.-D.; Lodriguito, M.; McGuire, M. J.; Kucharski, S. A.; Kuś, T.; Musiał, M. *Theor. Chem. Acc.* **2004**, *112*, 349–393.

- 28 Kowalski, K.; Piecuch, P. *J. Chem. Phys.* **2001**, *115*, 2966–2978.
- 29 Kowalski, K.; Piecuch, P. *J. Chem. Phys.* **2000**, *113*, 18–35.
- 30 Veis, L.; Antalík, A.; Brabec, J.; Neese, F.; Legeza, O.; Pittner, J. *J. Phys. Chem. Lett.* **2016**, *7*, 4072.
- 31 White, S. R.; Noack, R. M. *Phys. Rev. Lett.* **1992**, *68*, 3487–3490.
- 32 White, S. R. *Phys. Rev. Lett.* **1992**, *69*, 2863–2866.
- 33 White, S. R. *Phys. Rev. B* **1993**, *48*, 10345–10356.
- 34 White, S. R.; Martin, R. L. *J. Chem. Phys.* **1999**, *110*, 7127–4130.
- 35 Chan, G. K.-L.; Head-Gordon, M. *J. Chem. Phys.* **2002**, *116*, 4462–4476.
- 36 Legeza, Ö.; Röder, J.; Hess, B. A. *Phys. Rev. B* **2003**, *67*, 125114.
- 37 Legeza, Ö.; Noack, R.; Sólyom, J.; Tincani, L. In *Computational Many-Particle Physics*; Fehske, H., Schneider, R., Weisse, A., Eds.; Lecture Notes in Physics; Springer Berlin Heidelberg, 2008; Vol. 739; pp 653–664.
- 38 Marti, K. H.; Reiher, M. *Z. Phys. Chem.* **2010**, *224*, 583–599.
- 39 Chan, G. K.-L.; Sharma, S. *Annu. Rev. Phys. Chem.* **2011**, *62*, 465–481, PMID: 21219144.
- 40 Wouters, S.; Van Neck, D. *The Eur. Phys. J. D* **2014**, *68*.
- 41 Szalay, S.; Pfeffer, M.; Murg, V.; Barcza, G.; Verstraete, F.; Schneider, R.; Legeza, Ö. *Int. J. Quant. Chem.* **2015**, *115*, 1342.
- 42 Yanai, T.; Kurashige, Y.; Mizukami, W.; Chalupský, J.; Lan, T. N.; Saitow, M. *Int. J. Quantum Chem.* **2014**, *115*, 283–299.
- 43 Kurashige, Y.; Yanai, T. *J. Chem. Phys.* **2011**, *135*, 094104.
- 44 Freitag, L.; Knecht, S.; Angeli, C.; Reiher, M. *J. Chem. Theory Comput.* **2017**, *13*, 451–459.
- 45 Saitow, M.; Kurashige, Y.; Yanai, T. *J. Chem. Phys.* **2013**, *139*, 044118.
- 46 Neuscammen, E.; Yanai, T.; Chan, G. K.-L. *Int. Rev. Phys. Chem.* **2010**, *29*, 231–271.
- 47 Sharma, S.; Chan, G. *J. Chem. Phys.* **2014**, *141*, 111101.
- 48 Sharma, P.; Bernales, V.; Knecht, S.; Truhlar, D. G.; Gagliardi, L. *Chem. Sci.* **2019**, *10*, 1716–1723.
- 49 Faulstich, F. M.; Laestadius, A.; Kvaal, S.; Örs Legeza; Schneider, R. *arXiv* **2018**, 1802.05699.
- 50 Faulstich, F. M.; Máté, M.; Laestadius, A.; Csirik, M. A.; Veis, L.; Antalík, A.; Brabec, J.; Schneider, R.; Pittner, J.; Kvaal, S.; Örs Legeza, *Journal of Chemical Theory and Computation* **2019**, *15*, 2206–2220.
- 51 Veis, L.; Antalík, A.; Legeza, O.; Alavi, A.; Pittner, J. *J. Chem. Theory Comput.* **2018**, *14*, 2439.
- 52 Pulay, P. *Chem. Phys. Lett.* **1983**, *100*, 151.
- 53 Sæbø, S.; Pulay, P. *Chem. Phys. Lett.* **1985**, *113*, 914.
- 54 Foster, J. M.; Boys, S. F. *Rev. Mod. Phys.* **1960**, *32*, 300.
- 55 Pipek, J.; Mezey, M. G. *J. Chem. Phys.* **1989**, *90*, 4916.
- 56 Knizia, G. *J. Chem. Theory Comput.* **2013**, *9*, 4834–4843, PMID: 26583402.
- 57 Sæbø, S.; Pulay, P. *J. Chem. Phys.* **1987**, *86*, 914.
- 58 Sæbø, S.; Pulay, P. *J. Chem. Phys.* **1988**, *88*, 1984.
- 59 Hampel, C.; Werner, H.-J. *J. Chem. Phys.* **1996**, *104*, 6286.
- 60 Schütz, M.; Werner, H.-J. *J. Chem. Phys.* **2001**, *114*, 661.
- 61 Schütz, M. *Phys. Chem. Chem. Phys.* **2002**, *4*, 3941.
- 62 Werner, H.-J.; Schutz, M. *J. Chem. Phys.* **2011**, *135*, 144116.
- 63 Schütz, M. *J. Chem. Phys.* **2002**, *116*, 8772.
- 64 Kirstensen, K.; Ziółowski, M.; Jansík, B.; Kjærgaard, T.; Jørgensen, P. *J. Chem. Theory Comput.* **2011**, *7*, 1677.
- 65 Høyvik, I.-M.; Kristensen, K.; Jansík, B.; Jørgensen, P. *The Journal of Chemical Physics* **2012**, *136*, 014105.
- 66 Kobayashi, M.; Nakai, H. *J. Chem. Phys.* **2008**, *129*, 044103.
- 67 Stoll, H. *Chem. Phys. Lett.* **1992**, *191*, 548.
- 68 Rolik, Z.; Kallay, M. *J. Chem. Phys.* **2011**, *135*, 104111.
- 69 Fedorov, D. G.; Kitaura, K. *J. Chem. Phys.* **2005**, *123*, 134103.
- 70 Li, S.; Ma, J.; Jiang, Y. *J. Comp. Chem.* **2001**, *23*, 237.
- 71 Edmiston, C.; Krauss, M. *J. Chem. Phys.* **1965**, *42*, 1119.
- 72 Meyer, W. *Int. J. Quant. Chem.* **1971**, *5*, 341.
- 73 Meyer, W. *Theor. Chim. Acta* **1974**, *35*, 277.
- 74 Werner, H.-J.; Meyer, W. *Mol. Phys.* **1976**, *31*, 855.
- 75 Botschwina, P.; Meyer, W. *Chem. Phys.* **1977**, *20*, 43.
- 76 Rosmus, P.; Meyer, W. *J. Chem. Phys.* **1978**, *69*, 2745.
- 77 Ahlrichs, R.; Kutzelnigg, W. *Theor. Chim. Acta* **1968**, *10*, 377.
- 78 Ahlrichs, R.; Driessler, F.; Lischka, H.; Staemmler, V.; Kutzelnigg, W. *J. Chem. Phys.* **1975**, *62*, 1235.
- 79 Neese, F.; Hansen, A.; Liakos, D. G. *J. Chem. Phys.* **2009**, *130*, 114108.
- 80 Neese, F.; Hansen, A.; Liakos, D. G. *The Journal of Chemical Physics* **2009**, *131*, 064103.
- 81 Hansen, A.; Liakos, D. G.; Neese, F. *J. Chem. Phys.* **2011**, *135*, 214102.
- 82 Huntington, L. M. J.; Hansen, A.; Neese, F.; Nooijen, M. *J. Chem. Phys.* **2012**, *136*, 064101.
- 83 Riplinger, C.; Neese, F. *The Journal of Chemical Physics* **2013**, *138*, 034106.
- 84 Pinski, P.; Riplinger, C.; Valeev, E. F.; Neese, F. *The Journal of Chemical Physics* **2015**, *143*, 034108.
- 85 Riplinger, C.; Pinski, P.; Becker, U.; Valeev, E. F.; Neese, F. *The Journal of Chemical Physics* **2016**, *144*, 024109.
- 86 Saitow, M.; Becker, U.; Riplinger, C.; Valeev, E. F.; Neese, F. *The Journal of Chemical Physics* **2017**, *146*, 164105.
- 87 Werner, H.-J.; Knizia, G.; Krause, C.; Schwilk, M.; Dornbach, M. *J. Chem. Theory Comput.* **2015**, *11*, 484–507.
- 88 Menezes, F.; Kats, D.; Werner, H.-J. *The Journal of Chemical Physics* **2016**, *145*, 124115.
- 89 Schwilk, M.; Ma, Q.; Köppl, C.; Werner, H.-J. *Journal of Chemical Theory and Computation* **2017**, *13*, 3650–3675, PMID: 28661673.
- 90 Tew, D. P.; Hemlich, B.; Hättig, C. *J. Chem. Phys.* **2011**, *135*, 074107.
- 91 Helmich, B.; Hättig, C. *J. Chem. Phys.* **2013**, *139*, 084114.
- 92 Schmidt, B.; Helmich, B.; Hättig, C. *Mol. Phys.* **2013**, *111*, 2463.
- 93 Guo, Y.; Sivalingam, K.; Valeev, E. F.; Neese, F. *The Journal of Chemical Physics* **2016**, *144*, 094111.
- 94 Antony, J.; Grimme, S.; Liakos, D. G.; Neese, F. *J. Phys. Chem. A* **2011**, *115*, 11210.
- 95 Anoop, A.; Thiel, W.; Neese, F. *J. Chem. Theory Comput.* **2010**, *6*, 3137.
- 96 Liakos, D. G.; Neese, F. *J. Chem. Theory Comput.* **2011**, *7*, 1511.
- 97 Zade, S. S.; Zamoshchick, N.; Reddy, A. R.; Fridman-Marueli, G.; Sheberla, D.; Bendikov, M. *J. Am. Chem. Soc.* **2011**, *133*, 1083.
- 98 Kubas, A.; Brase, S.; ; Fink, K. *Chem. Eur. J.* **2012**, *18*, 8377.
- 99 Ashtari, M.; Cann, N. M. *J. Chromatogr. A* **2011**, *1218*, 6331.
- 100 Zhang, J.; Dolg, M. *Chemistry – A European Journal* **2014**, *20*, 13909–13912.

- ¹⁰¹ Minenkov, Y.; Chermak, E.; Cavallo, L. *Journal of Chemical Theory and Computation* **2015**, *11*, 4664–4676, PMID: 26574257.
- ¹⁰² Sparta, M.; Neese, F. *Chem. Soc. Rev.* **2014**, *43*, 5032–5041.
- ¹⁰³ Liakos, D. G.; Sparta, M.; Kesharwani, M. K.; Martin, J. M. L.; Neese, F. *Journal of Chemical Theory and Computation* **2015**, *11*, 1525–1539.
- ¹⁰⁴ Demel, O.; Pittner, J.; Neese, F. *J. Chem. Theory Comput.* **2015**, *11*, 3104–3114.
- ¹⁰⁵ Lang, J.; Švaňa, M.; Demel, O.; Brabec, J.; Kedžuch, S.; Noga, J.; Kowalski, K.; Pittner, J. *Mol. Phys.* **2017**, *115*, 2743–2754.
- ¹⁰⁶ Brabec, J.; Lang, J.; Saitow, M.; Pittner, J.; Neese, F.; Demel, O. *J. Chem. Theory Comput.* **2018**, *14*, 1370–1382.
- ¹⁰⁷ Lang, J.; Brabec, J.; Saitow, M.; Pittner, J.; Neese, F.; Demel, O. *Phys. Chem. Chem. Phys.* **2019**, *21*, 5022–5038.
- ¹⁰⁸ Moritz, G.; Reiher, M. *J. Chem. Phys.* **2007**, *126*, 244109.
- ¹⁰⁹ Boguslawski, K.; Marti, K. H.; Reiher, M. *J. Chem. Phys.* **2011**, *134*, 224101.
- ¹¹⁰ Adler, T.; Werner, H.-J. *J. Chem. Phys.* **2011**, *135*, 144117.
- ¹¹¹ Adler, T. B.; Werner, H.-J. *J. Chem. Phys.* **2009**, *130*, 241101.
- ¹¹² Legeza, Ö.; Veis, L.; Mosoni, T. QC-DMRG-Budapest, a program for quantum chemical DMRG calculations.
- ¹¹³ Neese, F. *WIREs Comput. Mol. Sci.* **2012**, *2*, 73–78.
- ¹¹⁴ Ivanic, J.; Collins, J. R.; Burt, S. K. *J. Phys. Chem. A* **2004**, *108*, 2314–2323.
- ¹¹⁵ Ghosh, D.; Hachmann, J.; Yanai, T.; Chan, G. K.-L. *J. Chem. Phys.* **2008**, *128*, 144117.
- ¹¹⁶ Zgid, D.; Nooijen, M. *J. Chem. Phys.* **2008**, *128*, 144116.
- ¹¹⁷ Yanai, T.; Kurashige, Y.; Ghosh, D.; Chan, G. K.-L. *Int. J. Quantum Chem.* **2009**, *109*, 2178–2190.
- ¹¹⁸ Dunning, T. H., Jr. *J. Chem. Phys.* **1989**, *90*, 1007–1023.
- ¹¹⁹ Woon, D.; T.H. Dunning, J. *J. Chem. Phys.* **1993**, *98*, 1358.
- ¹²⁰ Balabanov, N.; Peterson, K. *J. Chem. Phys.* **2005**, *123*, 064107.
- ¹²¹ Barcza, G.; Legeza, Ö.; Marti, K. H.; Reiher, M. *Phys. Rev. A* **2011**, *83*, 012508.
- ¹²² Fertitta, E.; Paulus, B.; Barcza, G.; Legeza, Ö. *Phys. Rev. B* **2014**, *90*, 245129.
- ¹²³ Legeza, Ö.; Sólyom, J. *Phys. Rev. B* **2003**, *68*, 195116.
- ¹²⁴ Legeza, Ö.; Röder, J.; Hess, B. *Phys. Rev. B* **2003**, *67*, 125114.
- ¹²⁵ Legeza, Ö.; Sólyom, L. *Phys. Rev. B* **2004**, *70*, 205118.
- ¹²⁶ Weigend, F.; Kohn, A.; Hattig, C. *J. Chem. Phys.* **2002**, *116*, 3175.
- ¹²⁷ Bross, D. H.; Hill, J. G.; Werner, H. J.; Peterson, K. A. *J. Chem. Phys.* **2013**, *139*, 094302.
- ¹²⁸ Pittner, J.; Nachtigall, P.; Čársky, P.; Hubač, I. *J. Phys. Chem. A* **2001**, *105*, 1354–1356.
- ¹²⁹ Bhaskaran-Nair, K.; Demel, O.; Šmydke, J.; Pittner, J. *J. Chem. Phys.* **2011**, *134*, 154106.
- ¹³⁰ Chattopadhyay, S.; Chaudhuri, R. K.; Mahapatra, U. S. *ChemPhysChem* **2011**, *12*, 2791–2797.
- ¹³¹ Pozun, Z. D.; Su, X.; Jordan, K. D. *J. Am. Chem. Soc.* **2013**, *135*, 13862–13869.
- ¹³² Demel, O.; Pittner, J.; Neese, F. *J. Chem. Theory Comput.* **2015**, *11*, 3104–3114.
- ¹³³ Veis, L.; Antalík, A.; Legeza, Ö.; Alavi, A.; Pittner, J. *Journal of Chemical Theory and Computation* **2018**, *14*, 2439–2445, PMID: 29570291.
- ¹³⁴ Zhang, W.; Loebach, J. L.; Wilson, S. R.; Jacobsen, E. N. *J. Am. Chem. Soc.* **1990**, *112*, 2801.
- ¹³⁵ Irie, R.; Noda, K.; Ito, Y.; Matsumoto, N.; Katsuki, T. *Tetrahedron Lett.* **1990**, *31*, 7345.
- ¹³⁶ Sears, J. S.; Sherrill, C. D. *J. Chem. Phys.* **2006**, *124*, 144314.
- ¹³⁷ Ma, D.; Li Manni, G.; Gagliardi, L. *J. Chem. Phys.* **2011**, *135*, 044128.
- ¹³⁸ Wouters, S.; Bogaerts, T.; Van Der Voort, P.; Van Speybroeck, V.; Van Neck, D. *J. Chem. Phys.* **2014**, *140*, 241103.
- ¹³⁹ Olivares-Amaya, R.; Hu, W.; Nakatani, N.; Sharma, S. *J. Chem. Phys.* **2015**, *142*, 034102.
- ¹⁴⁰ Stein, C. J.; Reiher, M. *J. Chem. Theory Comput.* **2016**, *12*, 1760.
- ¹⁴¹ Sharma, S.; Knizia, G.; Guo, S.; Alavi, A. *J. Chem. Theory Comput.* **2017**, *13*, 488.
- ¹⁴² Veis, L.; Antalík, A.; Brabec, J.; Neese, F.; Legeza, O.; Pittner, J. *J. Phys. Chem. Lett.* **2016**, *7*, 4072.
- ¹⁴³ Antalík, A.; Veis, L.; Brabec, J.; Legeza, Ö.; Pittner, J. *arXiv e-prints* **2019**, arXiv:1905.06833.

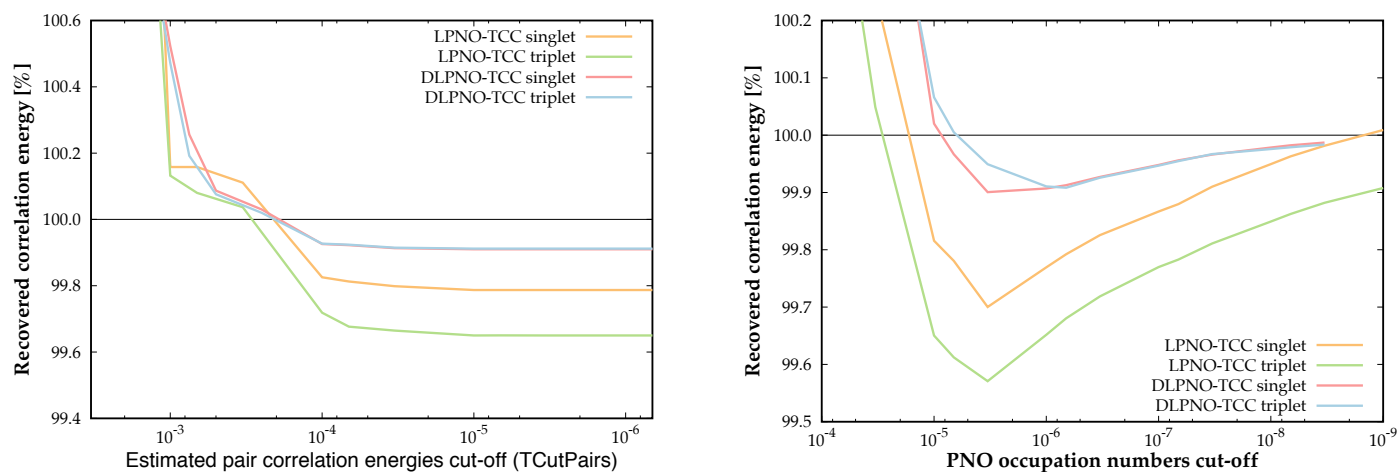


FIG. 3. The percentage of recovered canonical correlation energy for TME in the cc-pVTZ basis, averaged over all studied geometries with respect to the cut-off parameters T_{CutPairs} (left) and T_{CutPNO} (right).

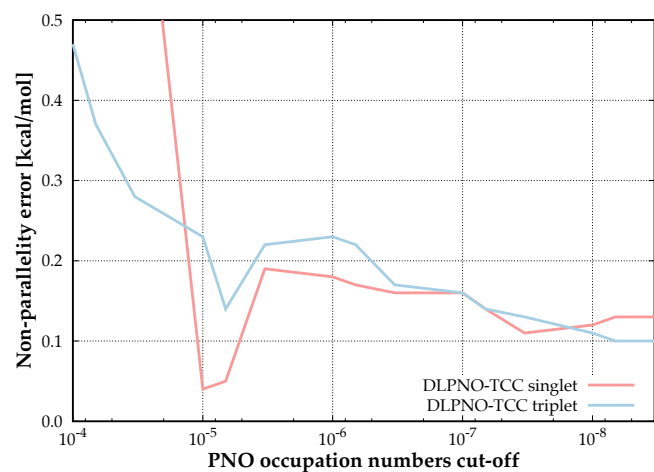


FIG. 4. The non-parallelity error for TME in cc-pVTZ as the function of T_{CutPNO} .

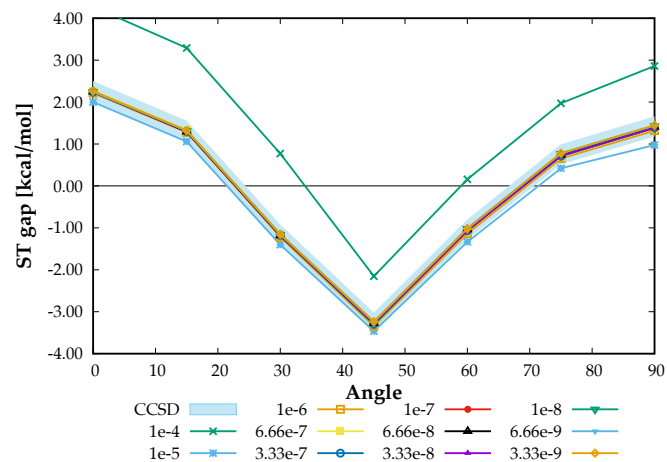


FIG. 5. The effect of T_{CutPNO} on the singlet-triplet gap of TME in the cc-pVTZ basis. The blue bar represents the canonical value ± 1 kJ/mol.

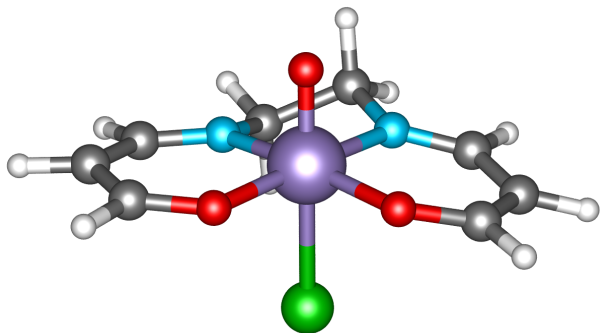
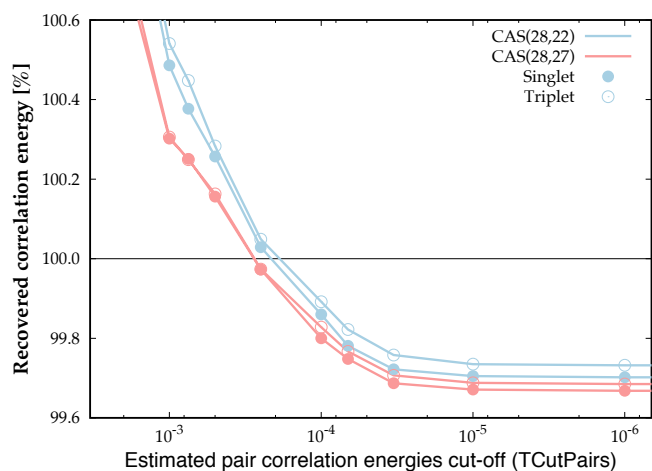
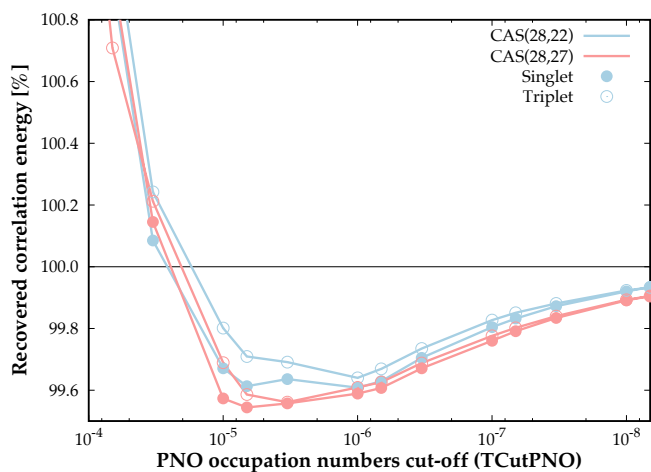
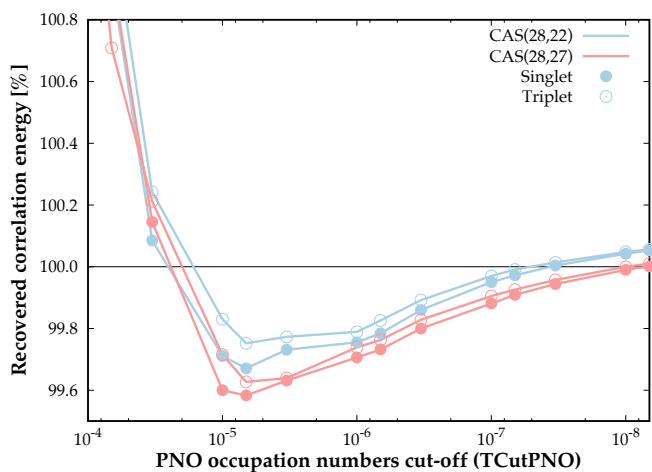


FIG. 6. A molecule of oxo-Mn(Salen)

FIG. 7. Dependence of the recovered correlation energy for singlet and triplet gap on T_{CutPairs} .FIG. 8. Dependence of the recovered correlation energy for singlet-triplet gap on T_{CutPNO} with $T_{\text{CutPairs}} = 1.0 \times 10^{-4}$ (left) and $T_{\text{CutPairs}} = 1.0 \times 10^{-5}$ (right).

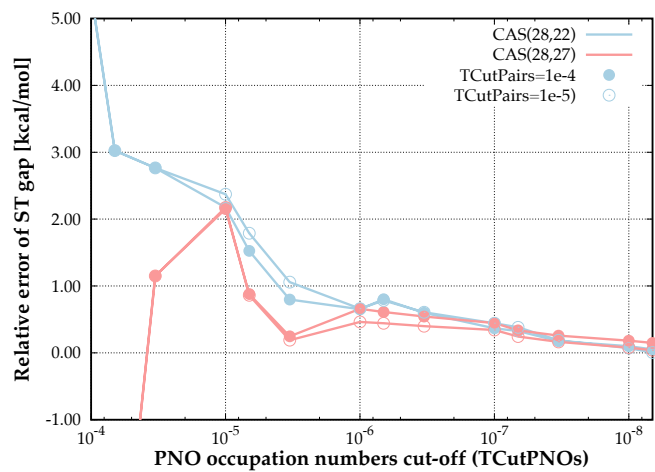


FIG. 9. Relative energy error of $\Delta E_{\text{ST}}^{\text{DLPNO-TCC}}$ with respect to the canonical value.